Chemical Science

EDGE ARTICLE

View Article Online
View Journal | View Issue

On the protonation of water†

A. Bodi,[a] J. Csontos,[b] M. Kállay,[b] S. Borkar[c] and B. Sztáray*[c]

Cite this: *Chem. Sci.*, 2014, **5**, 3057

Received 16th March 2014
Accepted 12th May 2014

DOI: 10.1039/c4sc00791c

www.rsc.org/chemicalscience

Imaging photoelectron photoion coincidence (iPEPICO) spectroscopy on isolated water molecules and water dimers establishes a new route to determining the water proton affinity (PA) with unprecedented accuracy. A floating thermochemical cycle constructed from the OH^+ and H_3O^+ appearance energies and three other spectroscopic values establishes the water PA as $683.2_2 \pm 0.2_5$ kJ mol^{-1} at 0 K, which converts to $688.8_1 \pm 0.2_5$ kJ mol^{-1} at room temperature. The experimental results are corroborated by a hierarchy of coupled-cluster calculations up to pentuple excitations and septuple-ζ basis set. Combined with diagonal Born–Oppenheimer and Dirac–Coulomb–Gaunt relativistic corrections, they provide the best theoretical estimate for both the hydronium ion's geometry and a water PA of 683.5 ± 0.4 kJ mol^{-1} and 689.1 ± 0.4 kJ mol^{-1} at 0 K and 298.15 K, respectively.

Introduction

The proton or, from a chemist's point of view, the hydrogen ion is omnipresent in chemistry and biochemistry. Proton-transfer reactions, typically coupled with electron transfer, are among the most fundamental processes in biological and chemical systems. Protonated species play a pivotal role in radiation chemistry, catalysis, surface chemistry, astrochemistry, and, to name a field close to our heart, mass spectrometry. In one of the experimental methods fueling the boom in proteomics, protein mass spectrometry, the gas-phase basicity of the different protonation sites on the peptide chain determines the structural information that can be deduced from the protein's fragmentation pattern. It is of little surprise, therefore, that much effort has been dedicated to determining proton affinities (PA, the enthalpy change upon protonation) or gas-phase basicities (GB, the Gibbs free-energy change upon protonation) in the past five decades.[1–9]

Water is a singularly important molecule in chemistry and in life sciences. Its protonation is one of the key chemical processes and the resulting hydronium ion is familiar to everyone who has ever taken a chemistry course. Hydronium, as an isolated ion, present in and enriching the chemistry of interstellar clouds and comet tails,[10] is an intriguing species in its own right. The plume ionosphere of Saturn's moon Enceladus is dominated by H_3O^+ and the absence of H_2O^+ indicates active proton-transfer chemistry.[11,12] Transient water vapor has also been recently observed at more than an order of magnitude higher flux (7000 kg s^{-1}) at the south pole of Europa, one of Jupiter's moons.[13] However, most of the observed water vapor is expected to fall back to Europa thanks to its larger escape velocity, whereas Enceladus' emissions may feed Saturn's ring and allow for ion chemistry to take place.

Hydronium ions are also abundant much closer to us: the ion chemistry of the stratosphere is governed by the hydronium ion and its water clusters.[14] Even closer, in the laboratory, chemical ionization techniques employ hydronium ions as the source of ionization; proton-transfer-reaction mass spectrometry (PTR-MS) is currently the standard reference technique to monitor the concentration of volatile organic compounds in the environment.[15] It is of little surprise, therefore, that the energetics of water protonation, *i.e.* the proton affinity of water, has been the subject of countless studies. In fact, the first ever published PA was that of water, by Tal'roze and Frankevich, in 1956.[1]

Most PA measurements nevertheless yield *relative* rather than absolute values. Absolute PAs can be established only for a few species if the enthalpy of formation of both M(g) and MH^+(g) are known. The proton affinities around and below the PA of water, and especially that of water, have always been problematic to determine.[9] The current standard compilation of PA values by Hunter and Lias lists water as an absolute PA anchor,[5] yet the recommended value is in fact taken from a relative PA measurement alone.[16] This mistake is then propagated into other publications, further exasperated by unit conversion errors.[7] Since the latest edition of the Hunter and Lias compilation,[5] at least two comprehensive studies were published to correct some of the inconsistencies.[7,9] In these works, the original water PA (or GB) value was revised by about the same amount, 2–3 kJ mol^{-1}, but in opposite directions and without reducing the error bars. Even if one of these values may

[a]*Molecular Dynamics Group, Paul Scherrer Institut, Villigen 5232, Switzerland*
[b]*MTA-BME Lendület Quantum Chemistry Research Group, Department of Physical Chemistry and Materials Science, Budapest University of Technology and Economics, Budapest 1521, Hungary*
[c]*Department of Chemistry, University of the Pacific, Stockton, CA 95211, USA. E-mail: bsztaray@pacific.edu*

† Electronic supplementary information (ESI) available: Fig. S1, Scheme S1 and Eqn (S1) illustrating the preferential dissociative photoionization model, and Tables S1–S4 on quantum chemistry results. See DOI: 10.1039/c4sc00791c

be right, it is impossible to say which, and it only appears sensible to assign a 3 kJ mol^{-1} uncertainty the water proton affinity, 691 ± 3 kJ mol^{-1}, as reported by Hunter and Lias.[5] This value agrees both in magnitude and in uncertainty with the proton affinity derived from literature photoionization data, based on the thermochemical cycle proposed herein. Together with newly measured and accurate dissociative photoionization thresholds of H-loss from water and, more importantly, OH-loss from the water dimer, it becomes possible to determine the water PA with less than tenth of this uncertainty.

Results

Imaging photoelectron photoion coincidence spectroscopy

Absolute proton affinities can be obtained if the heats of formation of both the precursor molecule and the protonated species are known from an internally consistent thermochemical compilation. By using imaging photoelectron photoion coincidence (iPEPICO) spectroscopy, it is possible to take a novel route: the proton affinity can be obtained directly from a floating thermochemical cycle, using two new iPEPICO results on water and the water dimer along with two well-known ionization energies, of the H and OH radicals (1312.050 kJ mol^{-1}, and 1255.947 ± 0.024 kJ mol^{-1}, respectively).[17,18] The fifth quantity that this new water PA determination relies on, as shown in the floating thermochemical cycle in Fig. 1, is the recently published water dimer dissociation energy by the Reisler group.[19] This water–water interaction energy of 13.22 ± 0.12 kJ mol^{-1} represented a significant leap in the accuracy of this quantity and it has been corroborated by high-level quantum-chemical calculations,[20] and the active thermochemical tables since its publication.[21] These three literature values together with the 0 K appearance energy of OH^+ from the dissociative photoionization of water and that of H_3O^+ from the water dimer, $(H_2O)_2$, yield the water proton affinity as:

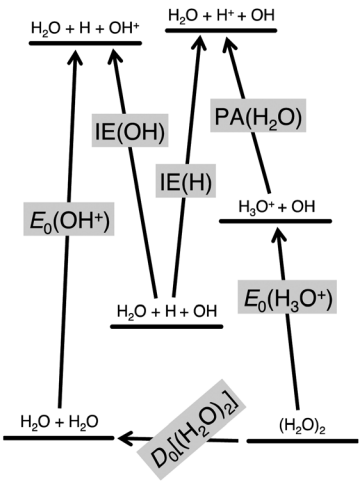

Fig. 1 Floating thermochemical cycle, not anchored to the standard scale of enthalpies of formation, used to derive the proton affinity of water. PA: proton affinity, IE: ionization energy, D_0: 0 K neutral dissociation energy, E_0: 0 K dissociative photoionization energy.

$$\mathrm{PA[H_2O]} = \mathrm{IE[H]} - \mathrm{IE[OH]} + D_0[(\mathrm{H_2O})_2] + E_0[\mathrm{OH^+}] - E_0[\mathrm{H_3O^+}] \quad (1)$$

Water and water dimer were measured using the iPEPICO experiment at the Swiss Light Source. Details of the technique,[22] the instrument,[23] and the VUV beamline[24] are given later. The following reactions occur in the dissociative photoionization of the two precursors:

$$\mathrm{H_2O} + h\nu \rightarrow \mathrm{H_2O^+} + \mathrm{e^-} \rightarrow \mathrm{OH^+} + \mathrm{H} + \mathrm{e^-} \quad (2)$$

$$(\mathrm{H_2O})_2 + h\nu \rightarrow (\mathrm{H_2O})_2{}^+ + \mathrm{e^-} \rightarrow \mathrm{H_3O^+} + \mathrm{OH} + \mathrm{e^-} \quad (3)$$

The fractional abundance of the parent and daughter ions plotted as function of photon energy, the breakdown curves, are shown in Fig. 2 and 3. Three different measurements were carried out to provide definitive threshold energies with close to 1 meV (0.1 kJ mol^{-1}) accuracy. Fig. 2a shows the room-temperature breakdown curve of water, while the two molecular beam measurements are plotted in Fig. 2b and c. First-order monochromatic light (that is, first-order diffraction from the monochromator grating) was used to obtain the data shown in Fig. 2b, and second-order light, with better resolution but less photon intensity yielded Fig. 2c.

The breakdown curves are modeled in terms of the parent ion's internal energy distribution to extract accurate 0 K dissociative photoionization thresholds. Briefly, the ion internal energy distribution can be approximated by transposing the neutral distribution onto the ion manifold. In a fast dissociation, ions with more internal energy than the dissociation barrier will dissociate, and the breakdown curve corresponds to the cumulative distribution function of the ion internal energy and, thus, is related to the neutral internal energy distribution at the experimental temperature and the 0 K appearance energy:

$$\mathrm{BD_p}(h\nu) = \int_0^{E_0-\mathrm{IE}} P_\mathrm{i}(E, h\nu)\mathrm{d}E \approx \int_0^{E_0-h\nu} P_\mathrm{n}(E)\mathrm{d}E \quad (4)$$

where $\mathrm{BD_p}$ is the parent ion fractional abundance, E_0 is the 0 K dissociative photoionization onset, IE is the adiabatic ionization energy, P_i is the internal energy distribution of the ion as a function of the photon energy, and P_n is the internal energy distribution of the neutral, calculated by the Boltzmann-formula. At $h\nu = E_0$, $\mathrm{BD_p}$ becomes 0, hence the disappearance energy of the parent yields directly the 0 K appearance energy. However, modeling the whole breakdown curve and varying the assumed E_0 for the best fit has proven to be more reliable and sometimes yields more insight into the underlying mechanism of dissociative photoionization. The PEPICO modeling technique and the computer code, proven in the analysis of over a hundred systems, has been described in more detail elsewhere.[25]

Preferential dissociative ionization model

The water breakdown curve model (broken lines in Fig. 2a), however, did not provide a satisfactory fit assuming that the H_2O room temperature internal energy distribution is shifted

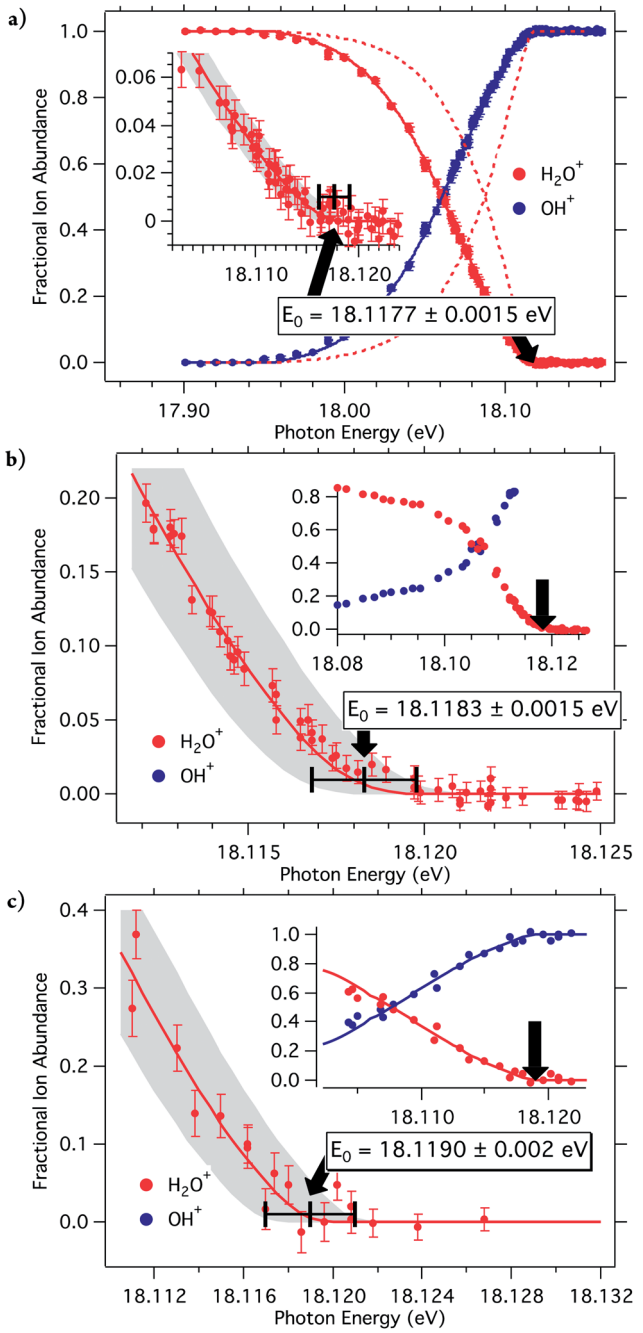

Fig. 2 iPEPICO breakdown curves corresponding to the $H_2O \rightarrow OH^+ + H + e^-$ dissociative photoionization process, (a) at room temperature, (b) in molecular beam with 1st order light, (c) in molecular beam with 2nd order light.

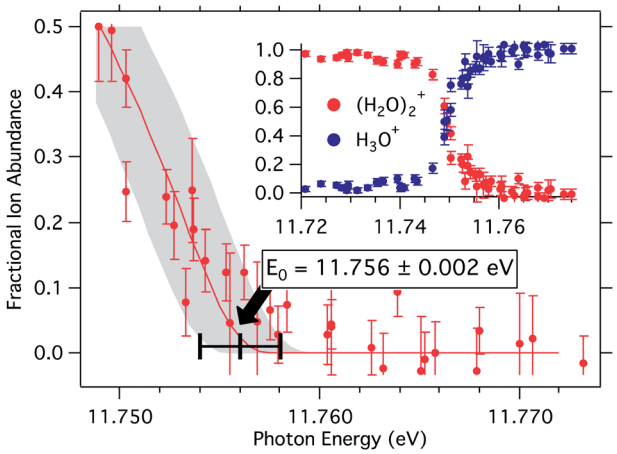

Fig. 3 Breakdown diagram for the dissociative photoionization of the water dimer: $(H_2O)_2 + h\nu \rightarrow H_3O^+ + OH + e^-$.

onto the ion manifold. This was briefly noted in the PFI-PEPICO water experiment by Ng *et al.*,[26] without further discussion as they did not attempt to model the breakdown curve, and accepted the disappearance energy of the parent ion as the 0 K onset. Examining the absolute coincidence counts shows that the OH^+ daughter ion signal and, as a result, the threshold photoelectron spectrum exhibit a sharp rise just before the dissociation onset (Fig. S1a in ESI†). As shown in Fig. S1b,† the rise of the TPES follows the cumulative internal energy distribution function, indicating that the threshold photoionization cross-section of water is larger when the sum of the photon energy and the internal energy of the water molecule exceeds the dissociative photoionization threshold. While at first glance such an effect, namely that the threshold photoionization cross-section is determined by the later fate of the photoion, may appear to run counter to causality, it actually provides a clue to the threshold photoionization mechanism. That is, it shows that an additional, intersystem crossing threshold photoionization channel opens up at the dissociation threshold, which is responsible for the increase in the threshold photoionization cross-section, probably decreasing the branching ratios of the various neutral decay channels.

The H-loss dissociative photoionization threshold lies in the energy range of the $\tilde{B}\ ^2B_2$ band in the TPES. Two electronic states correlate adiabatically with the ground state H + OH^+ products, therefore two pathways may lead to triplet OH^+ production at threshold.[27] The bound $\tilde{B}$ ion state either has to convert internally to the ground $\tilde{X}\ ^2B_1$ ion state, or it has to undergo intersystem crossing to the quartet $\tilde{a}\ ^4B_1$ state. The key to preferential dissociative threshold photoionization is the intersystem crossing path *via* the quartet electronic state, which only opens up at threshold. Thus, even if the total photoabsorption cross-section stays constant below and above threshold, an additional threshold photoionization decay channel leads to a higher threshold photoionization cross section, as illustrated by Scheme S1 in ESI.† By using a preferential dissociative photoionization factor to account for the resulting gain in the OH^+ signal, the modified version of eqn (4), given in ESI,† reproduces the shape of the breakdown curves well, shown by the solid lines in Fig. 1a.

The breakdown curve in Fig. 2a is, thus, fitted using room-temperature internal energy distribution of water, and a preferential dissociative ionization factor of 3.6, which agrees with the four-fold increase in the TPES signal at the onset. To extract accurate 0 K appearance energies from the molecular beam experimental data in Fig. 2b and c, the data points close to E_0 have been modeled by the same preferential dissociative

ionization factor. The three OH^+ appearance energies were determined to be 18.1177 ± 0.0015 eV, 18.1183 ± 0.0015 eV, and 18.119 ± 0.002 eV, for the three data sets in Fig. 2a–c, respectively. The largest contributor to the uncertainty in the first two values is the photon energy resolution as the signal-to-noise ratio is very good. In the case of the molecular beam measurement with second order light, the photon flux was much lower and uncertainty of 2 meV takes the lower signal-to-noise ratio into account. These three, independently obtained and calibrated values result in a reciprocal error-square weighted average[28] E_0 value of 18.1182 ± 0.0009 eV (1748.14 ± 0.09 kJ mol^{-1}). This agrees to within 0.2 meV with the sum of the water dissociation energy measured by Rizzo and Tennyson (41145.92 ± 0.12 cm^{-1}) and the OH ionization energy (104989 ± 2 cm^{-1}) of Wiedmann *et al.*,[17,29,30] *i.e.* 18.1184 eV.

The appearance energy of H_3O^+ from the water dimer was previously reported to be 11.73 ± 0.03 eV and more recently as 11.74 ± 0.05 eV.[31,32] Modeling the iPEPICO breakdown diagram with an optimized sample temperature of 60 K, as shown in Fig. 3, yields a significantly better defined appearance energy than possible hitherto, at $E_0 = 11.755_6 \pm 0.002$ eV ($1134.2_4 \pm 0.19$ kJ mol^{-1}).‡

With these two iPEPICO appearance energies, the water dimerization energy, and the ionization energies of H and OH, eqn (1) yields $683.2_2 \pm 0.2_5$ kJ mol^{-1} for the 0 K PA of water. The uncertainty of this value is based on the error bars cited or reported herein, assuming independent measurements and random error propagation. As shown in the quantum-chemistry section below, this converts to $688.8_1 \pm 0.2_5$ kJ mol^{-1} at 298.15 K, representing a significant correction of the literature value of 691 ± 3 kJ mol^{-1}, while also reducing its uncertainty by more than an order of magnitude.

Quantum chemistry

Great advances have been made in the field of computational thermochemistry in recent years, and quantum-chemical methods have evolved to a stage where the calculation of thermodynamic functions of small molecules is possible with an accuracy comparable to if not higher than that of the most accurate experimental methods. New experiments accurate to within a kJ mol^{-1} need to go hand-in-hand with quantum chemistry to provide a feedback loop and computational methods must be validated on ever more accurate experimental data before they are applied to experimentally inaccessible systems. In this work, we used a composite quantum-chemical approach to determine the proton affinity of water and, in the process, the structure of the water molecule and the hydronium ion, as well.

The molecular geometry of the isolated water molecule is well known, but few accurate measurements have been reported for the geometrical parameters of the hydronium ion and without firm and accurate computational support. Thus, we decided to calculate the equilibrium geometry of the hydronium ion and, for consistency, that of the water molecule, using the same composite model. Our results for the bond length and angle of the water molecule, 0.9577 ± 0.0002 Å and 104.48 ± 0.03°, respectively, agree with the experimental values[33] of 0.9575 Å and 104.51°. On the other hand, 0.9752 ± 0.0002 Å, and 111.96 ± 0.04° were obtained for the bond length and the H–O–H angle in the hydronium ion, respectively. These values, especially the bond angle, are considerably different from, but more accurate than the corresponding experimental results[34] of 0.974 ± 0.001 Å and 113.6 ± 0.1°. Therefore, the calculated geometries were used in the subsequent thermochemical calculations.

At the optimized geometries, energy calculations were performed with a composite model to evaluate the PA of water at 0 K, while thermal corrections were obtained using the standard tools of statistical thermodynamics using the computed rotational and vibrational energy levels. Our calculations yielded 683.5 ± 0.4 kJ mol^{-1}, and 689.1 ± 0.4 kJ mol^{-1} for the PA at 0 K, and 298.15 K, respectively, in near-perfect agreement with the measurements. From the latter value, and the calculated water[35,36] and hydronium ion entropies, 188.83 ± 0.04 J mol^{-1} K^{-1}, and 193.79 ± 0.40 J mol^{-1} K^{-1}, respectively, the gas-phase basicity of water was also determined as 658.0 ± 0.4 kJ mol^{-1} at 298.15 K.

Methods

Imaging photoelectron photoion coincidence spectroscopy

Water and water dimer were measured using the imaging photoelectron-photoion coincidence (iPEPICO) spectrometer[23] at the X04DB VUV beamline[24] of the Swiss Light Source (SLS). In the room-temperature measurement of water, the sample was evaporated into the iPEPICO apparatus through an effusive source. Typical pressures in the experimental chamber were less than 4×10^{-6} mbar during measurements. In the molecular beam measurements of cold isolated water molecules and water dimers, neon and argon, respectively, was saturated with room-temperature water and expanded into the source chamber from 0.8 bar through a 50 μm orifice. The pressure in the source chamber was kept below 2×10^{-4} mbar and it was under 6×10^{-6} mbar in the experimental chamber. The sample is ionized using monochromatic vacuum UV synchrotron radiation from the X04DB bending magnet beamline in a less than 2 × 2 mm interaction region. Photon energies are calibrated using Ar and Ne autoionization lines in first and second order. The photon energy resolution was better than 2 meV in the measurements with grating first order light. Electrons and ions are extracted and accelerated in opposite directions using a 120 V cm^{-1} constant electric field at the ionization spot. The field was varied between 20 and 120 V cm^{-1} in control experiments and the breakdown diagram was confirmed to be field independent. Electrons are velocity map imaged onto a DLD40 Roentdek position sensitive delay-line detector. At threshold, this detector has better than 1 meV kinetic energy resolution. Ions are detected in delayed coincidence with the photoelectrons by a Jordan TOF C-726 nonimaging microchannel plate detector after being analyzed by a two-stage Wiley–McLaren TOF mass spectrometer with a 5.5 cm long first and a 1 cm long second acceleration region, and a 55 cm drift region, satisfying space-focusing conditions.

The non-zero kinetic energy, "hot", electron contamination of the threshold electron signal at the center of the image was approximated by and subtracted from the center signal based on the average count rate in a ring area surrounding the center spot of the detector.[37] Electron hit times and positions and ion hit times were correlated using a multiple-start/multiple-stop data acquisition scheme.[38] With this technique, the photoions were internal energy-selected by correlating only the ions that were in delayed coincidence with the corrected threshold electron signal.

Quantum chemistry

Our models are based on the hierarchy of coupled-cluster (CC) methods,[39] which provide results smoothly convergent to the exact solution of the Schrödinger equation in the given atomic orbital basis set. These methods are combined with the correlation consistent basis sets of Dunning and co-workers,[40] which, together with basis set extrapolation techniques,[41] guarantee the systematic convergence of the energy and molecular properties to the non-relativistic infinite basis set limit in the framework of the Born–Oppenheimer approximation. The inclusion of post-Born–Oppenheimer and relativistic corrections then yields the most accurate and precise properties currently attainable for many-electron systems. Even though previous studies have rarely achieved the accuracy reported here, similar schemes have been successfully applied to determine thermodynamic and other molecular properties.[42,43] An in-depth discussion of the calculations is available elsewhere.[44]

The geometrical parameters (bond lengths and angles, hereafter denoted commonly by P) are evaluated as

$$P = P_{\mathrm{DKH/CCSD(T)}} + \Delta P_{\mathrm{T}} + \Delta P_{\mathrm{(Q)}} + \Delta P_{\mathrm{Q}}, \quad (5)$$

where $\Delta P_{\mathrm{T}} = P_{\mathrm{CCSDT}} - P_{\mathrm{CCSD(T)}}$, $\Delta P_{\mathrm{(Q)}} = P_{\mathrm{CCSDT(Q)}} - P_{\mathrm{CCSDT}}$, $\Delta P_{\mathrm{Q}} = P_{\mathrm{CCSDTQ}} - P_{\mathrm{CCSDT(Q)}}$, while $P_{\mathrm{DKH/CCSD(T)}}$ and $P_{\mathrm{CCSD(T)}}$, P_{CCSDT}, $P_{\mathrm{CCSDT(Q)}}$, and P_{CCSDTQ} are the corresponding parameters calculated with the CC singles, doubles, and perturbative triples [CCSD(T)], CC singles, doubles, and triples (CCSDT), CC singles, doubles, triples, and perturbative quadruples [CCSDT(Q)], and CC singles, doubles, triples, and quadruples (CCSDTQ) methods, respectively. In all calculations, the standard non-relativistic Hamiltonian was employed except for the evaluation of $P_{\mathrm{DKH/CCSD(T)}}$, for which the scalar relativistic Douglas–Kroll–Hess (DKH) Hamiltonian was used. To calculate the final estimate for a parameter, the contribution evaluated with the largest basis sets were considered. The error for a particular contribution was estimated as the difference of the aforementioned values and the values obtained with the second largest basis set; the error of the final parameter was calculated from these differences on the basis of Gauss's law. The intermediate results are listed in Tables S1–S4 of ESI.†

The proton affinity is computed as

$$\begin{aligned}\mathrm{PA} = {} & \mathrm{PA_{HF}} + \Delta\mathrm{PA_{MP2}} + \Delta\mathrm{PA_{CCSD}} + \Delta\mathrm{PA_{(T)}} + \Delta\mathrm{PA_{T}} + \Delta\mathrm{PA_{(Q)}} \\ & + \Delta\mathrm{PA_{Q}} + \Delta\mathrm{PA_{P}} + \Delta\mathrm{PA_{DBOC/CCSD}} + \Delta\mathrm{PA_{DBOC/T}} \\ & + \Delta\mathrm{PA_{DKH/HF}} + \Delta\mathrm{PA_{DKH/(T)}} + \Delta\mathrm{PA_{DC/HF}} + \Delta\mathrm{PA_{DC/(T)}} \\ & + \Delta\mathrm{PA_{DCG/HF}} + \Delta\mathrm{PA_{DCG/(T)}} + \Delta\mathrm{PA_{ZPE}}, \end{aligned} \quad (6)$$

where $\Delta\mathrm{PA_{MP2}} = \mathrm{PA_{MP2}} - \mathrm{PA_{HF}}$, $\Delta\mathrm{PA_{CCSD}} = \mathrm{PA_{CCSD}} - \mathrm{PA_{MP2}}$, $\Delta\mathrm{PA_{(T)}} = \mathrm{PA_{CCSD(T)}} - \mathrm{PA_{CCSD}}$, $\Delta\mathrm{PA_{T}} = \mathrm{PA_{CCSDT}} - \mathrm{PA_{CCSD(T)}}$, $\Delta\mathrm{PA_{(Q)}} = \mathrm{PA_{CCSDT(Q)}} - \mathrm{PA_{CCSDT}}$, $\Delta\mathrm{PA_{Q}} = \mathrm{PA_{CCSDTQ}} - \mathrm{PA_{CCSDT(Q)}}$, $\Delta\mathrm{PA_{P}} = \mathrm{PA_{CCSDTQP}} - \mathrm{PA_{CCSDTQ}}$, with $\mathrm{PA_X}$ standing for the PA calculated with method X, such as Hartree–Fock (HF), second-order Møller–Plesset (MP2), and CCSD(T) to CCSDTQP. $\Delta\mathrm{PA_{DBOC/T}} = \Delta\mathrm{PA_{DBOC/CCSDT}} - \Delta\mathrm{PA_{DBOC/CCSD}}$, where $\Delta\mathrm{PA_{DBOC/X}}$ is the contribution of the diagonal Born–Oppenheimer correction (DBOC) to the PA calculated with method X, $\Delta\mathrm{PA_{DKH/(T)}} = \Delta\mathrm{PA_{DKH/CCSD(T)}} - \Delta\mathrm{PA_{DKH/HF}}$, where $\Delta\mathrm{PA_{DKH/X}}$ is the scalar relativistic contribution to the PA evaluated with method X using the Douglas–Kroll–Hess Hamiltonian. The $\Delta\mathrm{PA_{DC/HF}}$, $\Delta\mathrm{PA_{DC/(T)}}$, $\Delta\mathrm{PA_{DCG/HF}}$, and $\Delta\mathrm{PA_{DCG/(T)}}$ symbols have similar meaning, except that they refer to incremental corrections, *i.e.* $\Delta\mathrm{PA_{DC/X}}$ is the difference of the PAs computed using the Dirac–Coulomb (DC) and DKH Hamiltonians with method X, and $\Delta\mathrm{PA_{DCG/X}}$ is the difference of the PAs obtained with the Dirac–Coulomb–Gaunt (DCG) and DC Hamiltonians. The final estimate for the PA is calculated based on the contributions evaluated with the largest basis sets. $\Delta\mathrm{PA_{ZPE}}$ is the difference of the zero point vibrational energy (ZPE) of the hydronium ion and water.

The ZPE as well as the temperature correction to the PA and the entropy of the molecules were calculated from literature data. The ZPE of water, 55.4865 kJ mol^{-1} (4638.31 cm^{-1}), was extracted from the highly accurate work of Csaszar *et al.*[45] The ro-vibrational partition function was calculated by explicit summation of the vibration-rotation energy levels published by Barber and co-workers.[35] The ZPE of H_3O^+, 89.1539 kJ mol^{-1} (7452.68 cm^{-1}), has been published by Halonen *et al.*[46] The rotational partition function was calculated utilizing the rigid-rotor approximation, while the vibrational partition function was computed by explicit summation using the vibrational levels reported in ref. 46. The translational contributions to the energy and entropy were calculated within the ideal gas approximation.

To estimate the error introduced by the use of the rigid rotor approximation in the case of H_3O^+, the thermal correction for NH_3 was calculated using the available vibration-rotation energy levels as well as invoking the rigid-rotor approximation and explicitly summing the experimental vibrational levels. The values differed by 12.5 J mol^{-1}. When comparing the available experimental frequencies with those of ref. 46, the error in the vibrational contribution for H_3O^+ can be estimated to be less than 9 J mol^{-1}. Therefore, a conservative estimate for the uncertainty in the thermal correction of H_3O^+ is 12.5 + 9 = 21.5 J mol^{-1}. Using the available vibration-rotation energy levels of NH_3, test calculations revealed an error of 0.21 J mol^{-1} K^{-1} introduced by the rigid-rotor approximation in the entropy value. Furthermore, the discrepancy between the experimental and *ab initio* geometry causes an error of 0.09 J mol^{-1} K^{-1} in the rotational contribution to the entropy of H_3O^+. The estimated effect on the vibrational contribution, due to the use of frequencies reported in ref. 46 is negligible at 0.06 J mol^{-1} K^{-1}. Hence, the uncertainty in the H_3O^+ entropy is estimated at 0.4 J mol^{-1} K^{-1}.

The quantum chemical calculations were carried out by the Molpro,[47] MRCC,[48] Dirac,[49] and Cfour[50] packages.

Conclusions

Solely spectroscopic data including new, imaging photoelectron photoion coincidence measurements on isolated water molecules and dimers, are used in a self-contained, floating thermochemical cycle to determine the absolute proton affinity of water an order of magnitude more accurately than has been possible for the last six decades. State-of-the-art quantum-chemical calculations are shown to keep pace with experiment, confirming the new, experimental proton affinity and also yielding the most accurate geometrical parameters for the hydronium ion. The absolute difference between the new experimental and quantum-chemical 0 K proton affinity values is less than 0.25 kJ mol^{-1}.

Acknowledgements

This work has been funded by the National Science Foundation (CHE-1266407), and by the European Research Council (ERC) under the European Community's Seventh Framework Programme (FP7/2007-2013), ERC Grant Agreement no. 200639. The financial support by the Swiss Department of Energy (BFE #100708), the American Chemical Society Petroleum Research Fund (PRF# 49930-ND6) and the Pacific Fund is also gratefully acknowledged. The experimental work was carried out at the VUV beamline of the Swiss Light Source of the Paul Scherrer Institut. The higher-order parallelized coupled-cluster calculations were run on the Hungarian HPC infrastructure (NIIF Institute, Hungary).

Notes and references

‡ The dissociative photoionization threshold of the water dimer lies at a higher energy than the Lyman-α line at 10.2 eV. Based on the SUMER data on the VUV spectrum of the sun,[51] the highest intensity peak in the solar spectrum towards the blue, namely the C III line at 97.7 nm (12.7 eV) is approx. 75 times weaker, which, assuming a photoionization cross section of 5 Mb, leads to water dimer dissociative photoionization rates of 2×10^{-7}, 3×10^{-8}, 1×10^{-9} and 4×10^{-10} s^{-1}, at the orbit of Mercury, Earth, Jupiter and Saturn, respectively, and means that water dimer is by and large stable with respect to dissociative photoionization in the interplanetary space.

1 V. L. Tal'roze and E. L. Frankevich, *Dokl. Akad. Nauk SSSR*, 1956, **111**, 376.
2 R. Yamdagni and P. Kebarle, *J. Am. Chem. Soc.*, 1976, **98**, 1320–1324.
3 T. B. McMahon and P. Kebarle, *J. Am. Chem. Soc.*, 1985, **107**, 2612–2617.
4 J. E. Szulejko and T. B. McMahon, *J. Am. Chem. Soc.*, 1993, **115**, 7839–7848.
5 E. P. L. Hunter and S. G. Lias, *J. Phys. Chem. Ref. Data*, 1998, **27**, 413–656.
6 T. B. McMahon, *Int. J. Mass Spectrom.*, 2000, **200**, 187–199.
7 M. Meot-Ner, *Int. J. Mass Spectrom.*, 2003, **227**, 525–554.
8 G. Czakó, E. Mátyus, A. C. Simmonett, A. G. Császár, H. F. Schaefer and W. D. Allen, *J. Chem. Theory Comput.*, 2008, **4**, 1220–1229.
9 I. Leito, I. A. Koppel, P. Burk, S. Tamp, M. Kutsar, M. Mishima, J.-L. M. Abboud, J. Z. Davalos, R. Herrero and R. Notario, *J. Phys. Chem. A*, 2010, **114**, 10694–10699.
10 J. M. Hollis, E. B. Churchwell, E. Herbst and F. C. De Lucia, *Nature*, 1986, **322**, 524–526.
11 T. E. Cravens, R. L. McNutt, J. H. Waite, I. P. Robertson, J. G. Luhmann, W. Kasprzak and W. H. Ip, *Geophys. Res. Lett.*, 2009, **36**, L08106.
12 R. L. Tokar, R. E. Johnson, T. W. Hill, D. H. Pontius, W. S. Kurth, F. J. Crary, D. T. Young, M. F. Thomsen, D. B. Reisenfeld, A. J. Coates, G. R. Lewis, E. C. Sittler and D. A. Gurnett, *Science*, 2006, **311**, 1409–1412.
13 L. Roth, J. Saur, K. D. Retherford, D. F. Strobel, P. D. Feldman, M. A. McGrath and F. Nimmo, *Science*, 2014, **343**, 171–174.
14 F. C. Fehsenfeld, I. Dotan, D. L. Albritton, C. J. Howard and E. E. Ferguson, *J. Geophys. Res.: Oceans*, 1978, **83**, 1333–1336.
15 L. Cappellin, T. Karl, M. Probst, O. Ismailova, P. M. Winkler, C. Soukoulis, E. Aprea, T. D. Märk, F. Gasperi and F. Biasioli, *Environ. Sci. Technol.*, 2012, **46**, 2283–2290.
16 B. J. McIntosh, N. G. Adams and D. Smith, *Chem. Phys. Lett.*, 1988, **148**, 142–148.
17 R. T. Wiedmann, R. G. Tonkyn, M. G. White, K. Wang and V. McKoy, *J. Chem. Phys.*, 1992, **97**, 768–772.
18 *CRC Handbook of Chemistry and Physics*, ed. H. W. Haynes, CRC Press, Boca Raton, 2013.
19 B. E. Rocher-Casterline, L. C. Ch'ng, A. K. Mollner and H. Reisler, *J. Chem. Phys.*, 2011, **134**, 211101–211104.
20 G. Czako, Y. Wang and J. M. Bowman, *J. Chem. Phys.*, 2011, **135**, 151102–151104.
21 B. Ruscic, *J. Phys. Chem. A*, 2013, **117**, 11940–11953.
22 T. Baer, B. Sztaray, J. Kercher, A. Lago, A. Bodi, C. Skull and D. Palathinkal, *Phys. Chem. Chem. Phys.*, 2005, **7**, 1507–1513.
23 A. Bodi, M. Johnson, T. Gerber, Z. Gengeliczki, B. Sztaray and T. Baer, *Rev. Sci. Instrum.*, 2009, **80**, 034101.
24 M. Johnson, A. Bodi, L. Schulz and T. Gerber, *Nucl. Instrum. Methods Phys. Res.*, 2009, **610**, 597–603.
25 B. Sztaray, A. Bodi and T. Baer, *J. Mass Spectrom.*, 2010, **45**, 1233–1245.
26 B. Ruscic, A. F. Wagner, L. B. Harding, R. L. Asher, D. Feller, D. A. Dixon, K. A. Peterson, Y. Song, X. Qian, C.-Y. Ng, J. Liu, W. Chen and D. W. Schwenke, *J. Phys. Chem. A*, 2002, **106**, 2727–2747.
27 A. G. Sage, T. A. A. Oliver, R. N. Dixon and M. N. R. Ashfold, *Mol. Phys.*, 2010, **108**, 945–955.
28 N. Shuman, L. Zhao, M. Boles, T. Baer and B. Sztaray, *J. Phys. Chem. A*, 2008, **112**, 10533–10538.
29 P. Maksyutenko, T. R. Rizzo and O. V. Boyarkin, *J. Chem. Phys.*, 2006, **125**, 181101–181103.
30 O. V. Boyarkin, M. A. Koshelev, O. Aseev, P. Maksyutenko, T. R. Rizzo, N. F. Zobov, L. Lodi, J. Tennyson and O. L. Polyansky, *Chem. Phys. Lett.*, 2013, **568–569**, 14–20.

31 C. Y. Ng, D. J. Trevor, P. W. Tiedemann, S. T. Ceyer, P. L. Kronebusch, B. H. Mahan and Y. T. Lee, *J. Chem. Phys.*, 1977, **67**, 4235–4237.
32 L. Belau, K. R. Wilson, S. R. Leone and M. Ahmed, *J. Phys. Chem. A*, 2007, **111**, 10075–10083.
33 K. L. Bak, J. Gauss, P. Jorgensen, J. Olsen, T. Helgaker and J. F. Stanton, *J. Chem. Phys.*, 2001, **114**, 6548–6556.
34 J. Tang and T. Oka, *J. Mol. Spectrosc.*, 1999, **196**, 120–130.
35 R. J. Barber, J. Tennyson, G. J. Harris and R. N. Tolchenov, *Mon. Not. R. Astron. Soc.*, 2006, **368**, 1087–1094.
36 M. W. Chase Jr, *J. Phys. Chem. Ref. Data*, 1998, **Monograph 9**, 1-1963.
37 B. Sztaray and T. Baer, *Rev. Sci. Instrum.*, 2003, **74**, 3763–3768.
38 A. Bodi, B. Sztaray, T. Baer, M. Johnson and T. Gerber, *Rev. Sci. Instrum.*, 2007, 78.
39 J. Gauss, in *Encyclopedia of Computational Chemistry*, ed. P. R. Schleyer, W. L. Jorgensen, H. F. Schaefer III, P. R. Schreiner and W. Thiel, Wiley, New York, 1998, p. 615.
40 D. E. Woon and J. T. H. Dunning, *J. Chem. Phys.*, 1995, **103**, 4572–4585.
41 A. Karton, P. R. Taylor and J. M. L. Martin, *J. Chem. Phys.*, 2007, **127**, 064104–064111.
42 A. Tajti, P. G. Szalay, A. G. Csaszar, M. Kallay, J. Gauss, E. F. Valeev, B. A. Flowers, J. Vazquez and J. F. Stanton, *J. Chem. Phys.*, 2004, **121**, 11599–11613.
43 M. Heckert, M. Kallay, D. P. Tew, W. Klopper and J. Gauss, *J. Chem. Phys.*, 2006, **125**, 044108–044110.
44 B. Csontos, B. Nagy, J. Csontos and M. Kállay, *J. Phys. Chem. A*, 2013, **117**, 5518–5528.
45 E. Matyus, G. Czako, B. T. Sutcliffe and A. G. Csaszar, *J. Chem. Phys.*, 2007, **127**, 084102–084113.
46 T. Rajamaki, A. Miani and L. Halonen, *J. Chem. Phys.*, 2003, **118**, 10929–10938.
47 MOLPRO is a package of *ab initio* programs written by H.-J. Werner, P. J. Knowles, G. Knizia, F. R. Manby and M. Schütz. Also see, *WIREs Comput. Mol. Sci.*, 2012, **2**, 242–253.
48 MRCC, a quantum chemical program suite written by M. Kállay, Z. Rolik, I. Ladjánszki, L. Szegedy, B. Ladóczki, J. Csontos, and B. Kornis. See also Z. Rolik, L. Szegedy, I. Ladjánszki, B. Ladóczki, and M. Kállay, *J. Chem. Phys.*, 2013, **139**, 094105 as well as: http://www.mrcc.hu.
49 DIRAC, a relativistic *ab initio* electronic structure program, Release DIRAC12 (2012), written by H. J. Aa. Jensen, R. Bast, T. Saue, and L. Visscher *et al.*, see http://www.diracprogram.org.
50 CFOUR, a quantum chemical program package written by J. F. Stanton, J. Gauss, M. E. Harding and P. G. Szalay, *et al.*, see http://www.cfour.de.
51 K. Wilhelm, U. Schuhle, W. Curdt, I. E. Dammasch, J. Hollandt, P. Lemaire and M. C. E. Huber, *ISSI Sci. Rep. Ser.*, 2002, **2**, 145.